A WIDER SEISMOGENIC ZONE AT CASCADIA DUE TO HYDROTHERMAL CIRCULATION IN SUBDUCTING OCEAN CRUST

by

Brian Dodd Cozzens

Submitted in partial fulfillment

of the requirements for the degree of

Master of Science in Hydrology

Department of Earth and Environmental Science

New Mexico Institute of Mining and Technology

Socorro, New Mexico, USA

June 2011

To Juliana Joy, for all the early mornings and late nights associated with our stay in the Land of Enchantment, and for being there for me always.

"I am haunted by waters."

-Norman Maclean, *A River Runs Through It*

ABSTRACT

Temperatures along subduction zone plate boundary faults have been used to estimate the area and extent of the seismogenic zone. Recent studies of the well-constrained Nankai margin of Japan show that hydrothermal circulation in the subducting crust cools the subduction zone and widens the area of the plate boundary fault that is between the key temperatures of 150 and 350 °C. Here, I present new thermal models for the Cascadia subduction zone that include the effects of fluid flow in the subducting crust. This fluid circulation cools the subduction zone and widens the thermally-defined seismogenic zone by shifting the intersection of the 350 °C isotherm within the plate boundary fault ~30 – 55 km landward. In contrast to the Nankai margin, the observed surface heat flux pattern for the thickly sedimented Cascadia margin provides only a weak constraint on subduction zone temperature. The tomographically-determined basalt-to-eclogite transition in the subducting slab is an additional constraint on the Cascadia subduction zone thermal models. The models most consistent with both the slab alteration observations and surface heat flux measurements include fluid circulation in an ocean crust aquifer with permeabilities of ~10^{-10} m^2, consistent with previous observations and inferences. This wider seismogenic zone is consistent with recent models of interseismic deformation. Estimates of co-seismic slip and ground shaking for a Cascadia megathrust earthquake based on a thermally-defined seismogenic zone should be revisited.

Keywords: Cascadia; seismogenic zone; hydrothermal circulation; episodic tremor and slip; ocean crust; permeability.

ACKNOWLEDGEMENTS

I am greatly indebted to many people who have helped me over the course of this project and my education. For the three years that I have known my wife, she has been my biggest supporter and best friend. She has made untold sacrifices for me and for us that I will never forget. My parents, Steve and Linda, have always encouraged me and helped me in any way that they could. I can't imagine better parents. Many of the faculty members at BYU–Idaho are wonderful examples of true teachers in everything they do. Specifically, Mark Lovell, Dan Moore, and Julie Willis exemplify the qualities that I wish to possess, not only as scientists, but also as human beings. My research advisor here at New Mexico Tech, Glenn Spinelli, is the epitome of professionalism and kindness. His ability to teach, motivate, and give confidence is uncanny. His help and guidance on this project were phenomenal. No one will ever be able to convince me that they had a better advisor in graduate school. My friends at New Mexico Tech and in the Socorro area have provided me with guidance, academic help, encouragement, and much needed diversion from the everyday hustle and bustle; for that I thank them. Carlos Ramírez-Torres and Katrina Koski, besides being great friends, are two of the best teachers in the department. Conversations with my committee members, Fred Phillips and Mark Person, have been helpful in both class and field applications, as well as in my research. The U.S. National Science Foundation and the U.S. Geological Survey supported this research.

TABLE OF CONTENTS

LIST OF TABLES

LIST OF FIGURES

INTRODUCTION

Approximately 90% of the total seismic moment release from 1900 to 1989 occurred within subduction zones [*Pacheco and Sykes*, 1992]. Subduction zone plate boundary faults are the primary location of large (>M 8) and tsunamigenic earthquakes [*Satake and Tanioka*, 1999]. Thus, there is considerable hazard associated with subduction zone seismicity. The position of the updip and downdip limits of seismicity along the plate boundary fault constrain the rupture width of large earthquakes and control the proximity of potentially damaging earthquakes to populated coastal areas. Throughout this thesis, I use "seismogenic zone" to describe the portion of the plate boundary fault that ruptures during large megathrust earthquakes and accumulates stress during interseismic periods. In a subduction zone, the width and location of the seismogenic zone is a key parameter for estimates of ground motion [*Cohee et al*., 1991].

Temperatures (and thermally- or kinetically-controlled mineral transitions) within subduction zones have been suggested as controls on the updip and downdip limits of seismicity [e.g., *Hyndman and Wang*, 1993; *Moore and Saffer*, 2001]. *Hyndman and Wang* [1993] developed the concept of the seismogenic portion of a subduction zone plate boundary fault extending from 150 – 350 ˚C. These temperatures are linked to key processes. The updip limit of seismicity (150 ˚C) was suggested to result from changes in frictional behavior and/or changes in fluid pressure associated with the smectite-illite transition [*Hyndman and Wang*, 1993;

Vrolijk, 1990]; more recent work suggests a host of diagenetic processes triggered at ~100 – 150 ˚C may control the updip limit [*Moore and Saffer*, 2001]. The downdip limit of seismicity is posited to occur at a transition from velocity weakening (below 350 ˚C) to velocity strengthening (above 350 ˚C) behavior, as determined in laboratory studies [e.g., *Blanpied et al*., 1991; *Blanpied et al.*, 1995]. From approximately 150 to 350 ˚C, fault zone materials are velocity weakening (Fig. 1). In velocity-weakening material, friction decreases during an episode of increased sliding velocity [*Scholtz*, 2002]. Below 150 ˚C and above 350 ˚C, fault rocks are

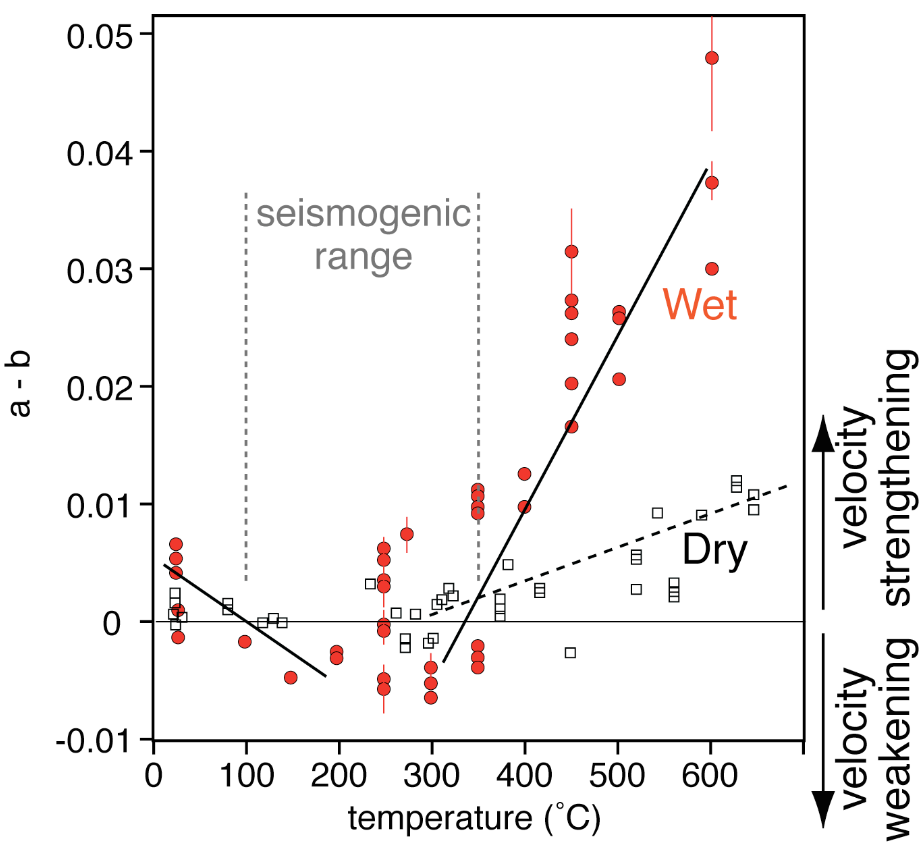

Figure 1: Relationship between velocity strengthening and velocity weakening in granite. Seismogenic zone shown from ~100 to 350 ˚C. a-b is the difference in the friction coefficient between slow and fast sliding velocity. Positive a-b equates to a higher friction coefficient for the fast velocity (velocity strengthening). Negative a-b equates to a lower friction coefficient for the fast velocity (velocity weakening). Modified from *Blanpied et al.* [1995].

velocity strengthening (i.e. friction increases during an episode of increased sliding velocity). Earthquakes can nucleate in velocity-weakening material, but not in velocity-strengthening material [*Scholtz*, 2002]. This led *Hyndman and Wang* [1993] to suggest that the key temperatures of 150 and 350 ˚C can be used to estimate the extent of the seismogenic zone for a subduction zone plate boundary fault. For the Cascadia subduction zone, the plate boundary fault is likely locked at the trench, as 150 ˚C (the warmest temperature commonly associated with the updip limit of seismicity) occurs seaward of the trench at the depth of the décollement. Therefore, the width of the seismogenic zone for Cascadia is controlled by the location of 350 ˚C on the plate boundary fault.

Estimating the extent of the seismogenic zone of the plate boundary fault for the Cascadia subduction zone has important implications for assessing the earthquake hazard in urban areas in the U.S. Pacific Northwest and southwestern Canada. On the Cascadia margin, the extent of the seismogenic zone is poorly resolved due to the lack of a large megathrust event during the instrumental record [*Rogers et al.*, 1996]. *Hyndman and Wang* [1993] developed thermal models for the Cascadia margin constrained by surface heat flux data and applied these thermal limits to estimate the extent of the seismogenic zone (Fig. 2). They note, however, that "a critical confirmation of the constraints on the seismogenic zone provided by thermal models is comparison with actual thrust earthquake data" [*Hyndman and Wang*, 1993]. Due to the dearth of instrumentally recorded megathrust earthquakes in the Cascadia subduction zone, verification of the constraints on the seismogenic zone provided by these original thermal models [*Hyndman and Wang*, 1993] is difficult.

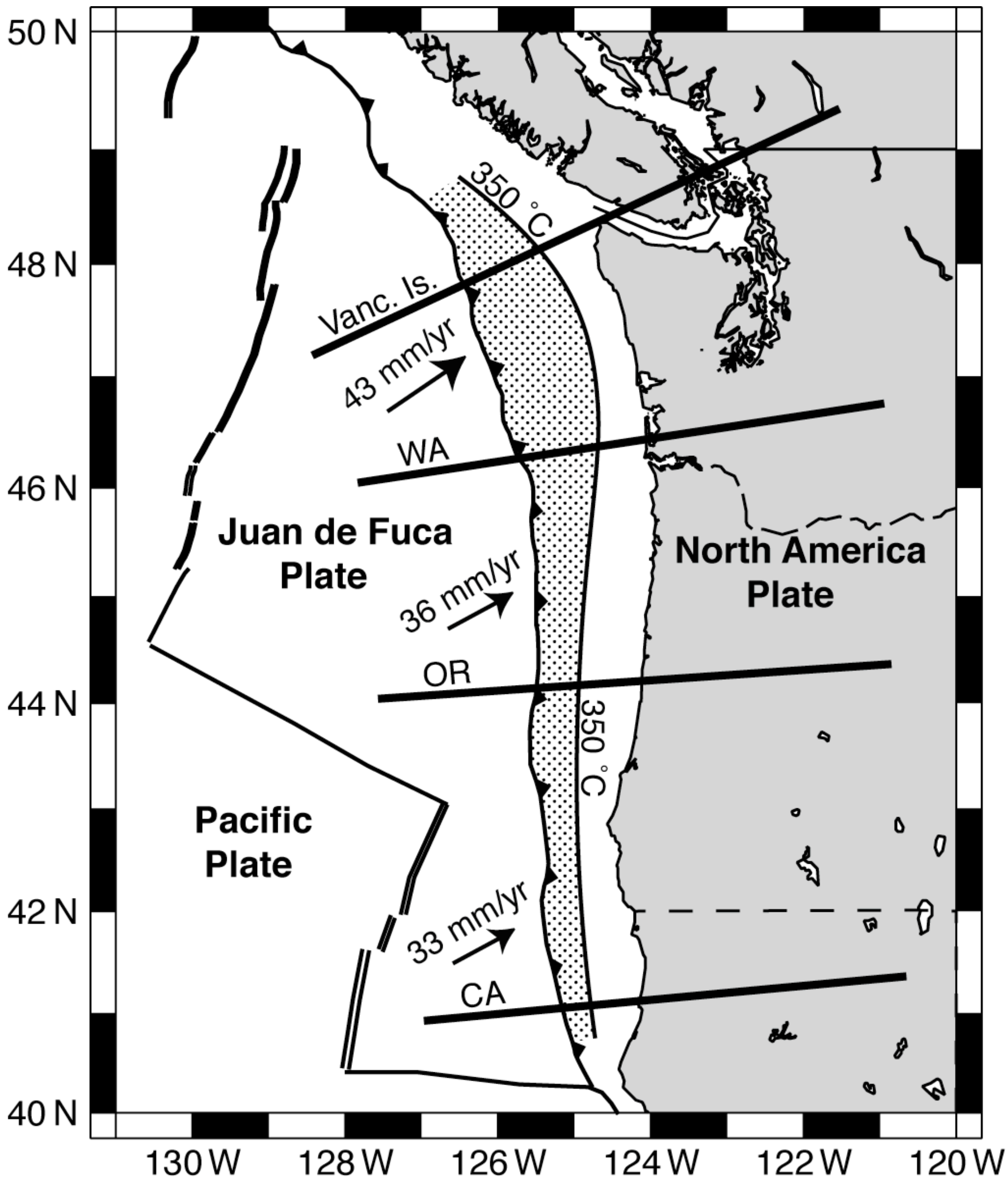

Figure 2: Map of the Cascadia subduction zone showing plate boundaries, the locations of four thermal model transects from this study, and the previously defined Cascadia megathrust seismogenic zone [*Hyndman and Wang*, 1993] (stippled). Arrows are convergence vectors along the margin.

Studies of the well-constrained Nankai margin of southern Japan show that the seismogenic portion of the plate boundary fault is between the key temperatures of 150 and 350 ˚C, and that hydrothermal circulation in the subducting crust cools the subduction zone, widening the portion of the plate boundary fault between 150 and 350 ˚C [*Spinelli and Wang*, 2008; *Spinelli and Wang*, 2009]. Thermal models that include the effects of fluid circulation in the subducting crust are consistent with observed surface heat-flux anomalies and the location of subducting slab alteration; models that do not include the thermal effects of fluid circulation are not consistent with these constraints [*Spinelli and Wang*, 2008; *Spinelli and Wang*, 2009].

Vigorous hydrothermal circulation in the highly-fractured, high-permeability ocean crust aquifer tends to homogenize temperatures [*Davis et al.*, 1997]. In a subduction zone, this circulation mines heat from the subducted crust and transports it seaward [*Kummer and Spinelli*, 2008]. The original thermal models for the Cascadia subduction zone [*Hyndman and Wang,* 1993], used to estimate the extent of the seismogenic zone [*Hyndman and Wang,* 1993] and in current hazard assessment [*Cohee et al*., 1991; *Silva et al*., 1996], do not include the effects of fluid circulation in the subducting ocean crust. I develop new thermal models for the Cascadia subduction zone that include the effects of fluid circulation in the subducting crust (Fig. 3). I use both surface heat flux observations and the location of the basalt-to-eclogite transition in the subducting slab to constrain the thermal models. These thermal models yield a new estimate for the potential rupture area for a Cascadia megathrust earthquake.

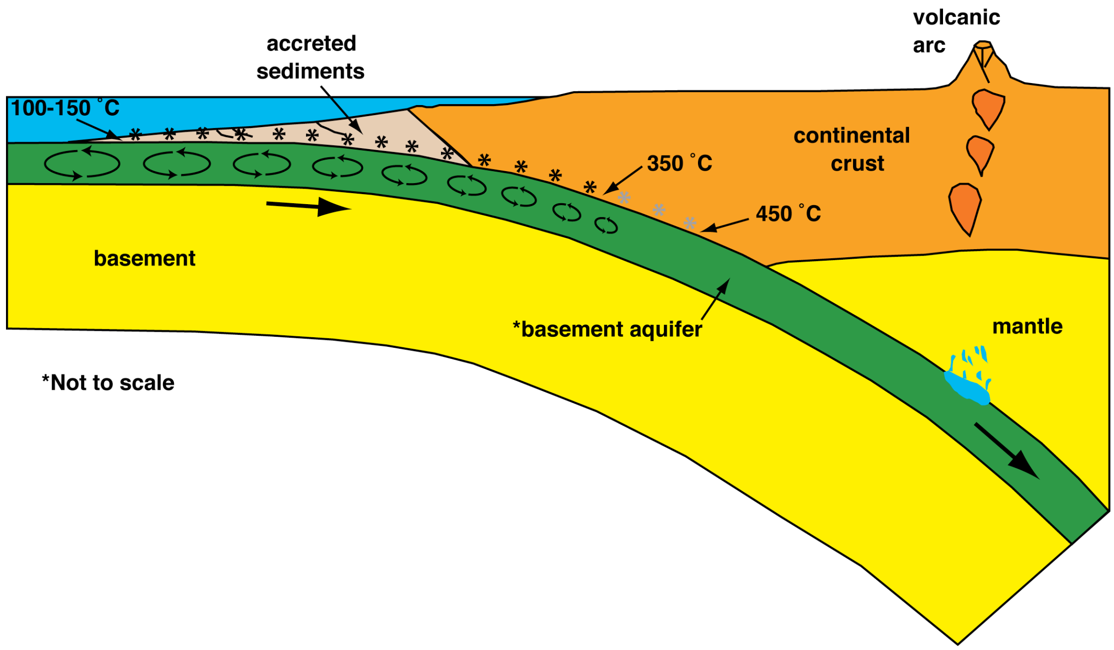

Figure 3: Cartoon cross-section showing hydrothermal circulation in the basement aquifer of oceanic crust. Basement aquifer is enlarged to show detail. In my models, fluid circulation (shown by convection cells in the basement aquifer) is only active in the subduction zone much shallower than the location of slab eclogitization (most circulation ceases by <25 km depth; eclogitization occurs at ~45 km depth). However, the continued subduction of hydrothermally cooled crust shifts the basalt-to-eclogite transition landward (Fig. 7).

METHODS

To estimate temperatures in the Cascadia subduction zone, I model heat generation and transport in four 2-D cross-sections through the margin (Fig. 2). I use a 2-D finite element heat transfer model [*Hyndman and Wang*, 1993; *Hyndman et al.*, 1995]. The thermal model accounts for heat production by plate boundary fault friction and radioactive decay, and for heat transport by conduction, advection of the subducting slab, mantle wedge flow, and vigorous fluid circulation in an ocean crust aquifer [*Spinelli and Wang*, 2008]. The governing heat transport equation used in this study is:

$$\nabla \bullet (K \nabla T) - \rho c v \bullet \nabla T + H = 0 ; \qquad (1)$$

where K is thermal conductivity, T is temperature, ρ is density, c is specific heat, ν is velocity of the subducting plate, H is sources of heat, and t is time. The first term in Equation 1 is heat transferred by conduction, the second term is advection of the subducting slab, and the third term is for heat sources or sinks. This model assumes the system is in steady-state and there is no thermally significant motion in the accretionary prism. In the governing equation, both solid material and fluid in pore space of the oceanic plate are advected at the convergence rate. The model does not include coupled fluid and heat transport; rather, I use a high Nusselt proxy to simulate the thermal effects of fluid circulation that is described below.

The ocean crust aquifer, composed of pillow basalt, comprises the upper ~600 m of igneous rock in the ocean crust [*Fisher*, 1998; *Fisher*, 2002]. Estimates for regional-scale ocean crust permeability are $10^{-10} – 10^{-9}$ m^2 (Fig. 4) [*Becker and Davis*, 2004]. For comparison to commonly encountered terrestrial lithologies, Tables 1 and 2 show permeability ranges for unconsolidated sediment [*Fetter*, 1994] and rocks [*Freeze and Cherry*, 1979]. The range of permeability for "permeable basalt" [*Freeze and Cherry*, 1979] overlaps values for well-sorted gravel [*Fetter*, 1994]. In this extremely permeable ocean crust aquifer, hydrothermal circulation is vigorous (possibly chaotic), even with the fairly small driving forces available resulting from modest temperature-controlled density differences in the ocean crust aquifer distant from large heat sources at mid-ocean ridges [*Davis and Becker*, 2002; *Fisher*, 2004].

It can be difficult to achieve numerical stability in models of coupled fluid and heat transport for these systems with extremely permeable basement rocks. In

Material	**Permeability (m^2)**
Clay	$10^{-18} – 10^{-15}$
Silt, sandy silts, clayey sands, till	$10^{-15} – 10^{-13}$
Silty sands, fine sands	$10^{-14} – 10^{-12}$
Well-sorted sands, glacial outwash	$10^{-12} – 10^{-10}$
Well-sorted gravel	$10^{-11} – 10^{-9}$

Table 1: Range of values of permeability for unconsolidated sediments. Modified from Fetter [1994].

Rock	**Permeability (m^2)**
Unfractured metamorphic and igneous rocks	$10^{-21} – 10^{-17}$
Shale	$10^{-20} – 10^{-16}$
Sandstone	$10^{-17} – 10^{-13}$
Limestone and dolostone	$10^{-16} – 10^{-13}$
Fractured metamorphic and igneous rocks	$10^{-15} – 10^{-11}$
Permeable basalt	$10^{-14} – 10^{-9}$
Karst limestone	$10^{-13} – 10^{-9}$

Table 2: Range of values of permeability for rocks. Modified from Freeze and Cherry [1979].

addition, the direction of fluid flow in such models is sensitive to the initial conditions [*Spinelli and Fisher*, 2004]. In such high permeability systems, the efficiency of convective heat transfer is very high; Nusselt number (*Nu*) greater than 100 [*Davis et al.*, 1997; *Spinelli and Fisher*, 2004; *Kummer and Spinelli*, 2008; *Spinelli and Wang*, 2008].

In systems with hydrothermal circulation vigorous enough to have *Nu* in excess of 20, a high-conductivity proxy for the thermal effects of the fluid circulation

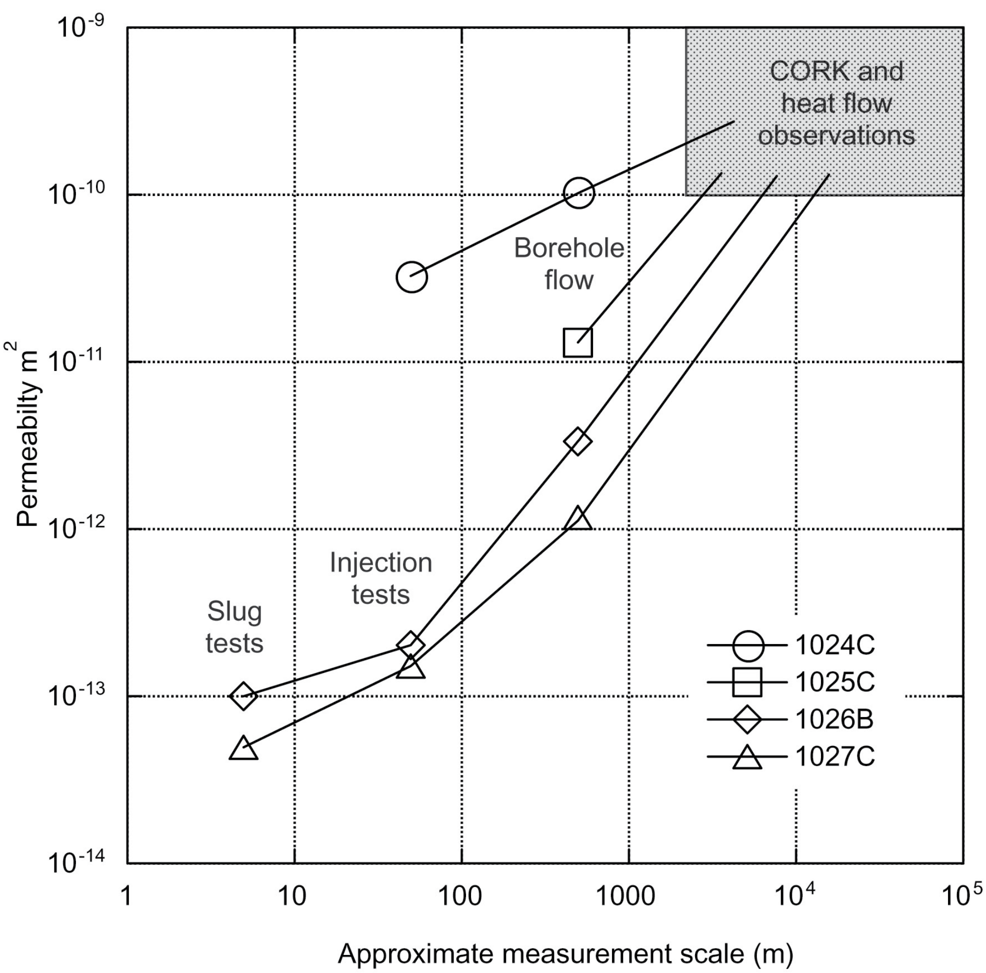

Figure 4: Measured and inferred permeabilities versus approximate scale for Juan de Fuca Ridge flank ocean crust. Stippled area shows range of values examined in this study. Modified from *Becker and Davis* [2004].

is accurate [*Davis et al.*, 1997]. This inspired *Spinelli and Wang* [2008] to use such a proxy to adapt a general subduction zone thermal model to include the effects of vigorous circulation in the ocean crust aquifer. This approach has been applied to thermal models for subduction zones offshore Japan [*Spinelli and Wang*, 2008] and Costa Rica [*Harris et al.*, 2010].

I use the same high-conductivity proxy in developing new thermal models for the Cascadia margin. In this approach, a Raleigh number (*Ra*) is defined for each aquifer element using the permeability, temperature-dependent fluid density and viscosity, and local heat flux:

$$Ra = \frac{\alpha g k L^2 \rho_f q}{\mu \kappa K}; \tag{2}$$

where α is fluid thermal expansivity, g is gravity, k is permeability, L is aquifer thickness, ρ_f is fluid density, q is conductive heat flux, μ is fluid viscosity, κ is thermal diffusivity, and K is thermal conductivity. An elemental *Nu*, quantifying the local efficiency of convective heat transfer, is derived from *Ra* using the empirical *Ra-Nu* relationship (Equation 3) found by comparing results from a coupled fluid and heat transport simulation to a conductive proxy of the same problem [*Kummer and Spinelli*, 2008; *Spinelli and Wang*, 2008].

$$Nu = 0.08Ra^{0.89} \tag{3}$$

The *Ra-Nu* relationship in Equation 3 is within the range of the host of published *Ra-Nu* relationships [*Wang*, 2004]. Multiplying the intrinsic thermal conductivity of the aquifer by *Nu* simulates the thermal effects of hydrothermal circulation. Because of nonlinear feedbacks between temperature and *Nu*, an iterative procedure is used.

Starting with a temperature field found using a conductive model (i.e., no fluid circulation; $Nu = 1$), a convergent solution (temperature variation of <1 ˚C in each element) is obtained usually within 10 iterations. I do not consider the small fluid sources due to dehydration reactions in the slab. They are important for fluid flow only if the permeability is extremely low, in which case the slow fluid flow is not thermally significant.

I model subduction zone temperatures with and without fluid circulation in the aquifer. For the simulations with fluid circulation, I explore a range of aquifer permeabilities. In all cases aquifer permeability decreases with burial depth (Fig. 6, inset), simulating the chemical and mechanical sealing of fractures as the ocean crust is progressively altered and compacted throughout subduction. I run simulations with pre-subduction aquifer permeability of 10^{-10}, $2x10^{-10}$, and 10^{-9} m^2, spanning the range of regional-scale ocean crust permeability [*Becker and Davis*, 2004].

For each of the four transects examined (Fig. 2), the geometry of the subduction zone is constrained by seismic reflection, refraction, and tomographic data (Fig. 5) [*Fuis*, 1998; *Gerdom et al*., 2000; *Parsons et al.*, 1998; *Flueh et al.*, 1998; *Gullick et al.*, 1998; *Nicholson et al.*, 2005; *Abers et al.*, 2009; *Rondenay et al.*, 2008]. Values for the thermal conductivity and radiogenic heat generation rate for the different lithologies in the models are shown in Table 3. Surface heat flux observations provide the primary constraint for most subduction zone thermal models. In addition to those data (Fig. 6) [*Hyndman and Wang*, 1993; *Hyndman and Wang*, 1995; *Trehu*, 2006; *Booth-Rea et al.*, 2008], I use the seismically observed location of the basalt-to-eclogite transition in the subducting crust [*Nicholson et al.*, 2005; *Abers et al.*, 2009; *Rondenay et al.*, 2008] to constrain our thermal models (Fig.

8). I determine the pressure-temperature (P-T) conditions in the center of the modelled subducting crust (3 km below the top of the basaltic basement rock) under various hydrologic conditions (Fig. 7). This is the first study to use the tomographically-determined basalt-to-eclogite transition to constrain a subduction zone thermal model. I use a phase diagram for mid-ocean ridge basalt [*Hacker et al.*, 2003] and the modelled P-T conditions to determine the depth at which the modelled subducting crust experiences eclogite metamorphism (Fig. 7). That depth is then compared to the observed depth of slab eclogitization to find the permeability trend that best fits the observation (Fig. 8).

Geologic Unit	**K [W m^{-1} K^{-1}]**	**Q [μW m-^{3}]**	**ρc [J m^{-3} K^{-1}]**
Sediment	1.15	0.6	2.5 x 10^{6}
Accretionary prism	1.15 - 2.0	0.6	2.5 x 10^{6}
Crescent terrane	1.8	0.05	2.5 x 10^{6}
Siletz terrane	1.8	0.05	2.5 x 10^{6}
Continental crust	2.0 - 2.5	0.2 - 0.6	2.5 x 10^{6}
Mantle wedge	3.1	0	2.5 x 10^{6}
Oceanic basement (including aquifer)	2.9	0	3.3 x 10^{6}

Table 3: Material properties used in finite element model. Geologic units can be seen in Fig. 5. The parameters K, Q, and ρc are thermal conductivity, radiogenic heat generation rate, and volumetric heat capacity (product of density and specific heat), respectively.

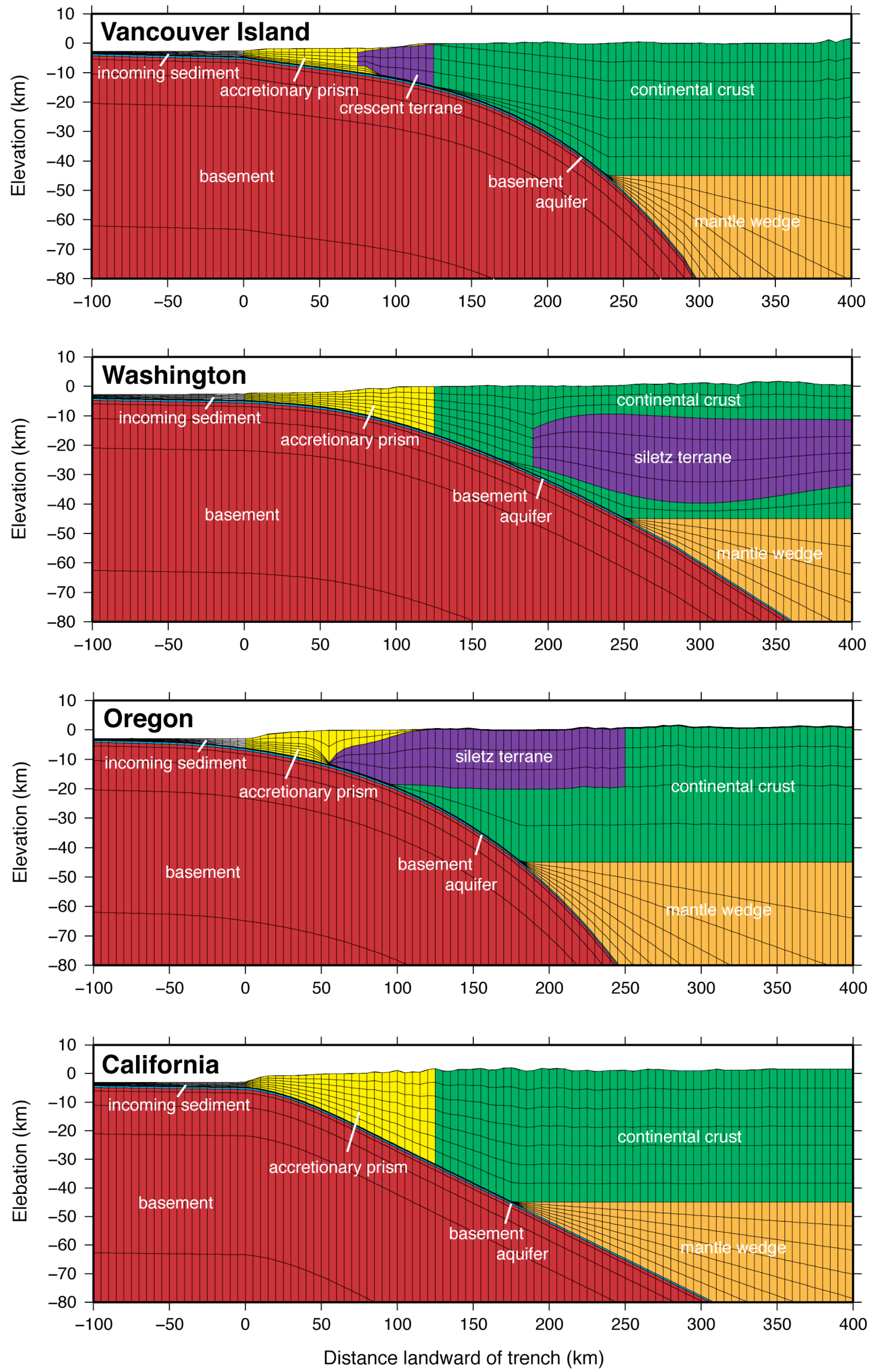

Figure 5: Cross-sectional view of the four thermal model transects in this study showing 2-D finite element grid spacing and discretization. Corresponding group properties can be seen in Table 3.

RESULTS

In the regions with most of the surface heat flux observations, on the incoming plate and margin wedge within ~40 km of the trench, modelled surface heat flux provides little to discriminate among many of the scenarios examined (Fig. 6).

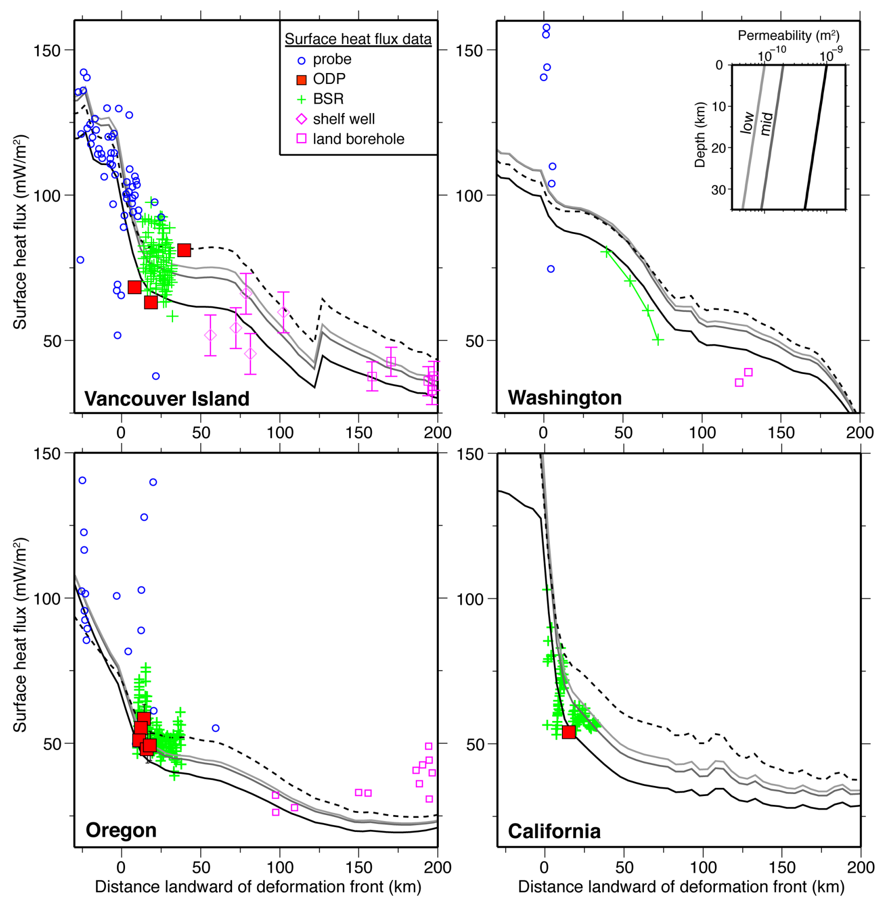

Figure 6: Measured and modelled surface heat flux along the four transects shown in Fig. 2. Dashed lines are modelled heat flux with no fluid circulation in the ocean crust. Solid lines are modelled surface heat flux with fluid circulation; inset shows ocean crust permeability trends, line weights and shading are keyed to model results. Observations are from seafloor probe measurements, temperature gradients in Ocean Drilling Program (ODP) and land boreholes, and estimates from the depth to a gas hydrate related bottom simulating reflector (BSR).

For the California transect, models with fluid circulation are more consistent with the observed surface heat flux than a model with no fluid circulation; however, each of the three models with different permeability trends reasonably approximates the data, with little to discriminate between them. For the Oregon, Washington, and Vancouver Island transects, modelled heat flux in all of the scenarios examined passes through the scattered data; the scatter in the data may reflect local advection and/or venting of fluid and heat. Because comparison of the modelled and observed surface heat flux is largely equivocal, the location of the basalt-to-eclogite transition for the subducting crust is a critical constraint on the thermal state of the Cascadia margin, except at the California transect where no tomographic profile is available at present.

Subduction of hydrothermally cooled crust shifts the basalt-to-eclogite transition farther landward than would be predicted with no fluid flow. Shear-wave velocity anomalies highlight the transition from hydrated basaltic crust to eclogitized material in the subducting slab for the Vancouver Island [*Nicholson et al.*, 2005], Washington [*Abers et al.*, 2009], and Oregon [Rondenay et al., 2008] transects (Fig. 8). In each case, slab eclogitization occurs at ~45 km depth; this is farthest inland for the shallowly dipping slab in the Washington transect and farther seaward for the steeply dipping slabs in the Vancouver Island and Oregon transects. Thermal models without the effects of fluid circulation in the ocean crust predict slab eclogitization at ~41, 38, and 42 km depth for the Vancouver Island, Washington, and Oregon transects, respectively (Fig. 7, Fig. 8). Including fluid circulation with the lowest permeability trend examined shifts the modelled slab eclogitization to ~45 km depth for Vancouver Island and Washington, and to 50 km depth for Oregon.

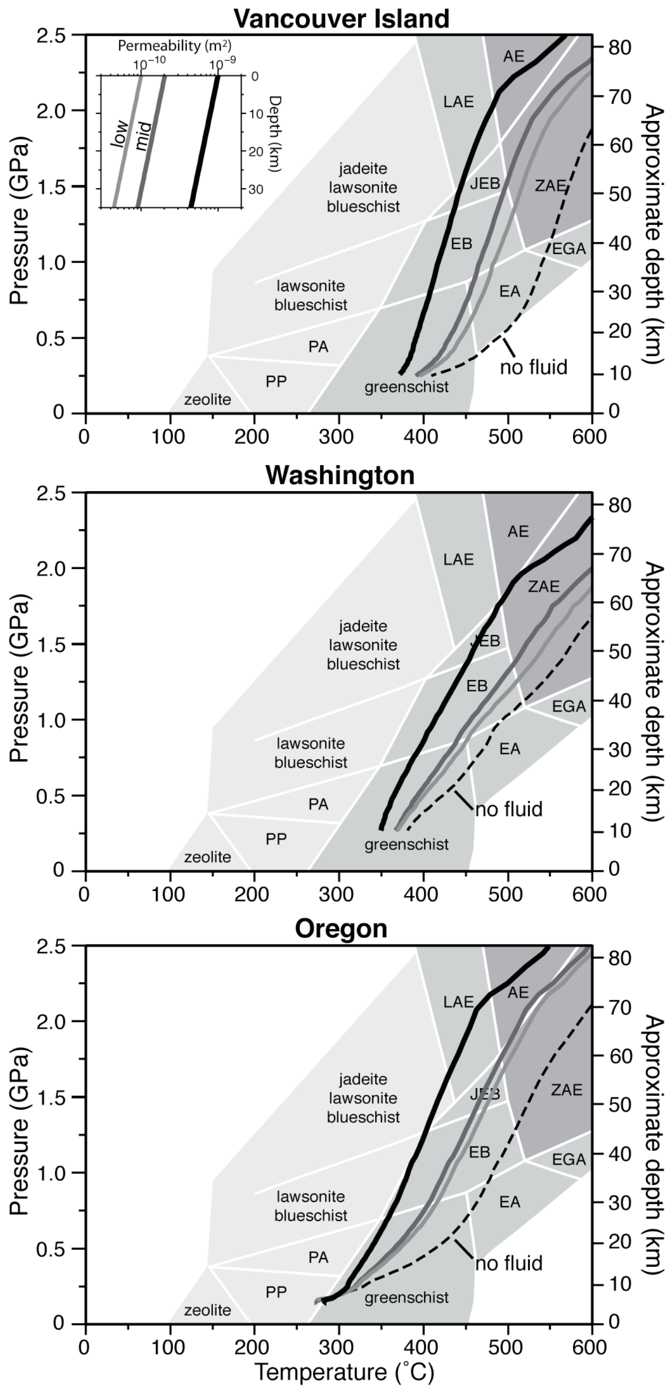

Figure 7: Pressure-temperature (P-T) paths for the center of the subducting crust (3 km below top of basaltic basement rock). These paths are overlain on a phase diagram showing metamorphic facies for mid-ocean ridge basalt [*Hacker et al.*, 2003]. We compare the location at which the modelled P-T paths enter the eclogite facies (ZAE or AE) to the tomographically observed location of slab eclogitization. Dashed lines are from models with no fluid circulation. Darker shading indicates lower water content in slab [*Hacker et al.*, 2003].

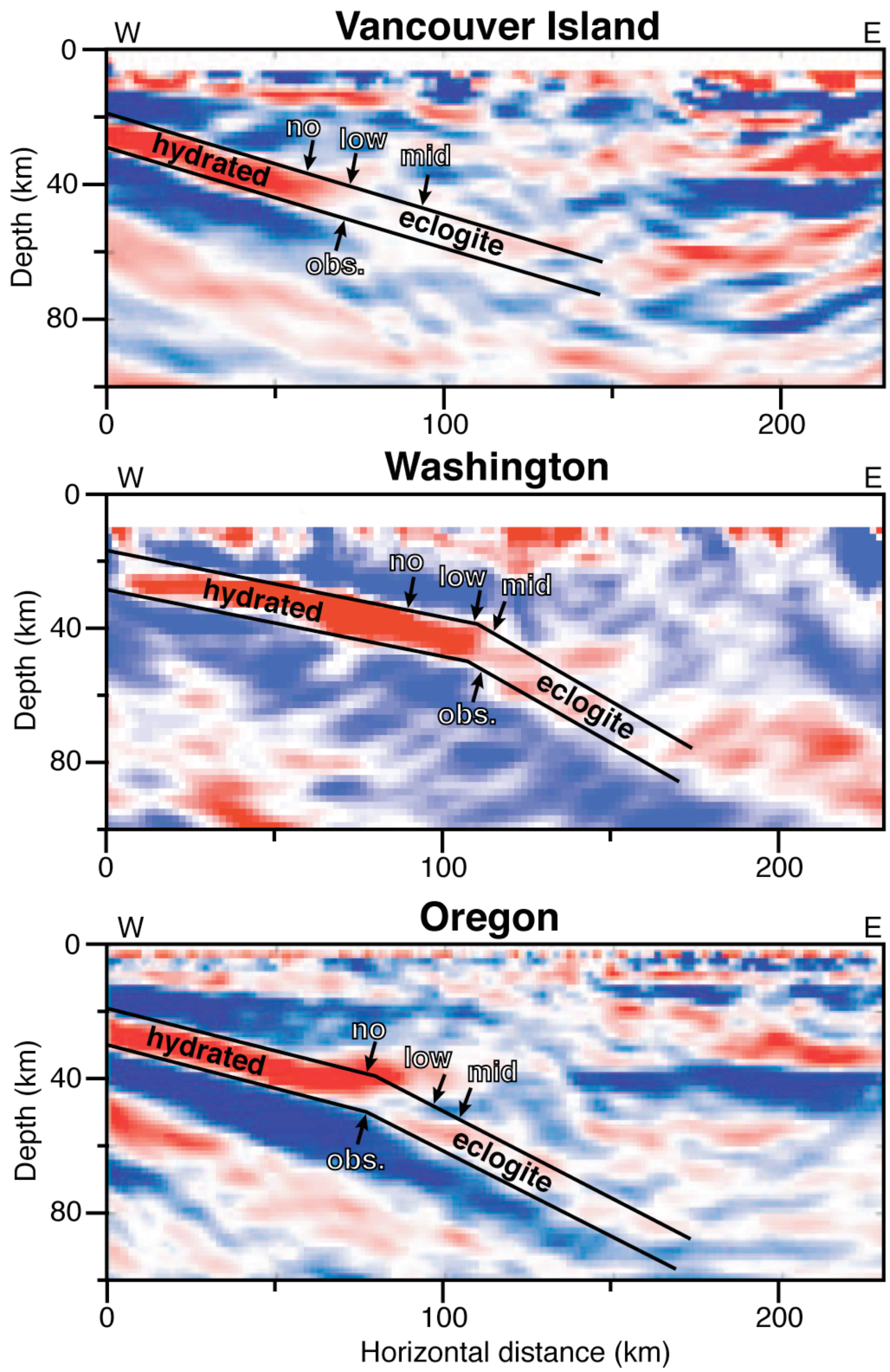

Figure 8: Scattered wave inversion cross-sections for Vancouver Island [*Nicholson et al.*, 2005], Washington [*Abers et al.*, 2009], and Oregon transects [*Rondenay et al.*, 2008]. Red indicates slow S-wave velocity; blue indicates fast S-wave velocity (range is ±10% relative to a background model for Vancouver Island and Oregon, ±5% for Washington). The locations at which the slab is expected to undergo eclogitization for thermal models with no fluid flow and hydrothermal circulation in ocean crust with the low and intermediate permeability trends (Fig. 6, inset) are indicated by ticks labeled no, low, and mid, respectively.

In selecting preferred thermal models for each transect, I choose the warmest (i.e. lowest permeability, least hydrothermally cooled) scenario for each transect consistent with the seismically observed basalt-to-eclogite transition location and the surface heat flux observations. Thus, I use the models with the lowest permeability ocean crust for Vancouver Island, Washington, and California transects; I use the no fluid flow model for the Oregon transect. This yields a conservative (i.e. smallest) thermally-defined seismogenic zone for the Cascadia subduction zone that extends ~30 – 55 km farther landward than earlier estimates, with the downdip limit of seismicity under much of the coastline along Washington (Fig. 9).

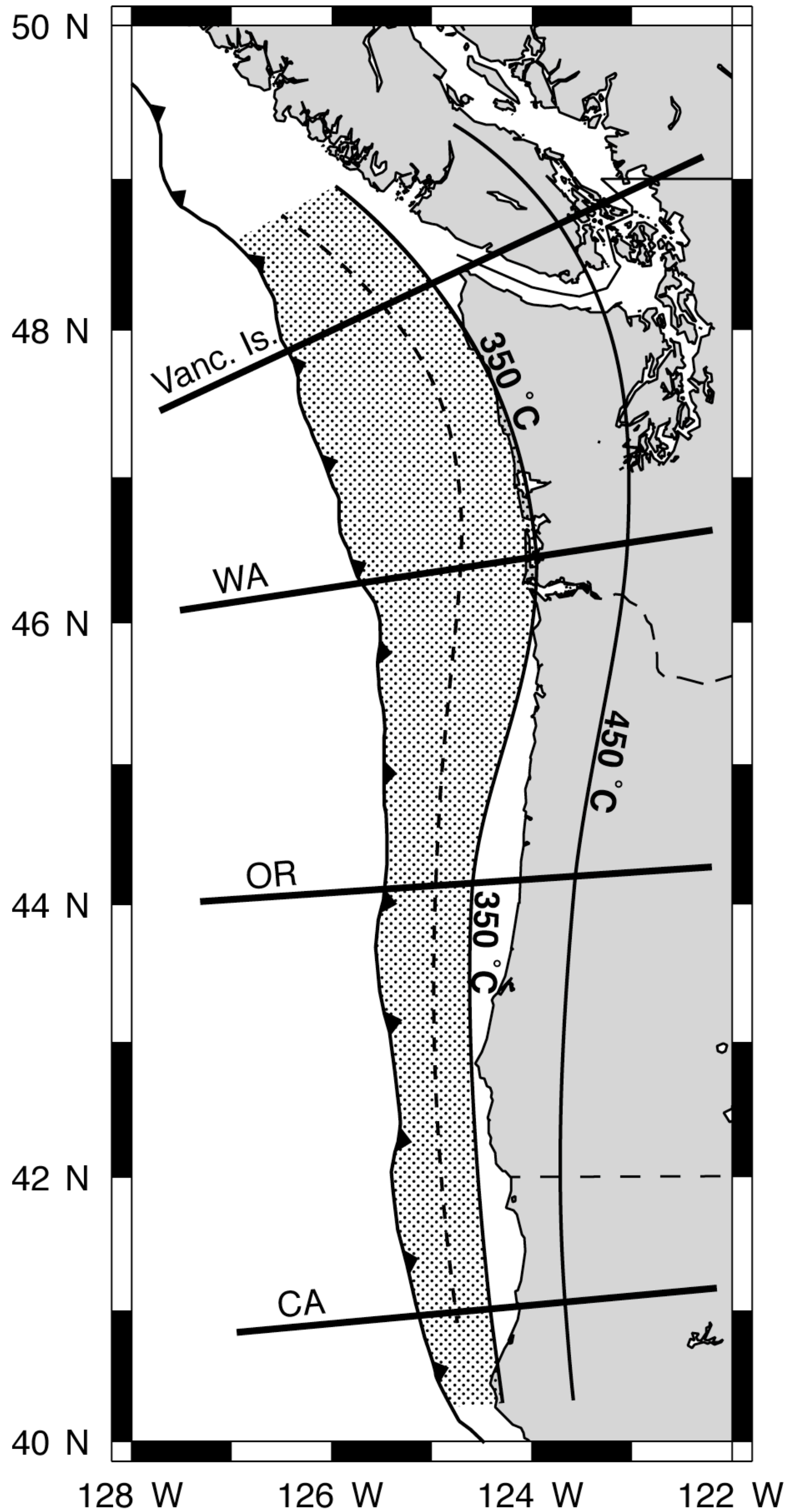

Figure 9: Map of Cascadia subduction zone with probable megathrust seismogenic zone, portion of plate boundary fault from 150 – 350 ˚C, stippled. The seismogenic zone extends up to 55 km farther landward than previously estimated [*Hyndman and Wang*, 1993] (dashed line), including under the coastline of Washington.

CONCLUSIONS

For the preferred models, the permeability of the subducting ocean crust aquifer (and therefore the vigour of hydrothermal circulation) is lower than estimated for either the Nankai [*Spinelli and Wang*, 2008; *Spinelli and Wang*, 2009] or Costa Rica [*Harris et al.*, 2010] margins. This difference may result from regional-scale permeability anisotropy for the ocean crust aquifer, with structurally-controlled high permeability parallel to the mid-ocean ridge axis [*Fisher et al.*, 2008]. On the Nankai and Costa Rica margins, magnetic lineations in the ocean crust are nearly perpendicular to the trench [*Spinelli and Wang*, 2008; *Harris et al.*, 2010]. This orientation of the high permeability direction in the ocean crust aquifer could facilitate hydrothermal circulation exchanging heat between the subducted and incoming ocean crust. Magnetic lineations for the incoming plate on the Cascadia margin are oblique to the trench offshore Vancouver Island; they transition to sub-parallel to the trench offshore Oregon [*Wilson*, 1993]. This is consistent with less hydrothermal heat extraction from the subducted crust for the Cascadia margin than for Nankai or Costa Rica. In addition, this could explain why there may be less hydrothermal cooling for the Oregon transect than for Vancouver Island and Washington transects. Subduction of older ocean crust offshore Oregon (~9 Ma) than offshore Vancouver Island (~7 Ma) may also limit the effect of hydrothermal cooling in the Oregon transect, given a trend for decreasing ocean crust aquifer permeability with increasing crustal age [*Becker and Davis*, 2004]. Our temperature estimates for the Oregon transect are slightly lower than previous estimates [*Hyndman and Wang*, 1993] due to our use of updated margin geometry [*Gerdom et al.*, 2000] and convergence rate [*McCaffrey et al.*, 2007] data; this temperature difference is small relative to the large shifts due to hydrothermal cooling for the Vancouver Island and Washington transects (Fig. 9).

New thermal models for the Cascadia margin consistent with surface heat flux data and the observed locations of subducting slab alteration indicate that hydrothermal circulation cools the subduction zone and widens the portion of the plate boundary fault between 150 and 350 ˚C. Thus, a potential rupture area extending farther landward should be considered in estimating ground shaking for a Cascadia megathrust earthquake. This wider seismogenic zone is consistent with recent models of interseismic locking on the plate interface and episodic tremor and slip (ETS) [*McCaffrey*, 2009; *Chapman and Melbourne*, 2009]. These models envision ETS occurring on the plate boundary fault downdip of the seismogenic zone. The downdip edge of the thermally-defined seismogenic zone is within ~25 km of the region of ETS in the Vancouver Island and Washington transects [*Rogers and Dragert*, 2003] and within ~70 – 90 km of the ETS region in southern Cascadia [*Boyarko and Brudzinski*, 2010]. For Vancouver Island, Washington, and Oregon, our thermal estimates indicate temperatures on the plate boundary fault at the updip end of the episodic tremor and slip region of 375 – 420 ˚C; temperatures at the downdip end are 500 – 550 ˚C. In the California transect, where younger (~5 Ma) warmer lithosphere is subducting, the plate interface in the ETS region is warmer, ~500 – 575 ˚C. These new temperature estimates may help shed light the processes controlling ETS.

REFERENCES

Abers, G. A., MacKenzie, L. S., Rondenay, S., Zhang, Z., Wech, A. G. & Creager, K. C. Imaging the source region of Cascadia tremor and intermediate-depth earthquakes. *Geology*, **37**, 1119-1122 (2009).

Becker, K. & Davis, E. E. in *Hydrogeology of the Ocean Lithosphere* (eds Davis, E. E. & Elderfield, H.) 189-224 (Cambridge University Press, New York, 2004).

Blanpied, M. L., Lockner, D. A. & Byerlee, J. D. Frictional slip of granite at hydrothermal conditions. *J. Geophys. Res*., **100**, 13045-13064 (1995).

Booth-Rea, G., Klaeschen, D., Grevemeyer, I. & Reston, T. Heterogeneous deformation in the Cascadia convergent margin and its relation to thermal gradient (Washington, NW USA). *Tectonics.*, **27**, TC4005 (2008).

Boyarko, D. C. & Brudzinski, M. R. Spatial and temporal patterns of nonvolcanic tremor along the southern Cascadia subduction zone, *J. Geophys. Res*., **115**, B00A22 (2010).

Chapman, J. S. & Melbourne, T. I. Future Cascadia megathrust rupture delineated by episodic tremor and slip. *Geophys. Res. Lett.*, **36**, L22301 (2009).

Cohee, B. P., Somerville, P. G. & Abrahamson, N. A. Simulated ground motions for hypothesized M_w=8 subduction earthquakes in Washington and Oregon. *Bull. Seismol. Soc. Amer.*, **81**, 28-56 (1991).

Davis, E. E., & Becker, K. Observations of natural state fluid pressures and temperatures in young oceanic crust and inferences regarding hydrothermal circulation, *Earth Planet. Sci. Lett.*, **204**, 231–248 (2002).

Davis, E. E., Wang, K., He, J., Chapman, D., Villinger, H. & Rosenberger, A. An unequivocal case for high Nusselt number hydrothermal convection in sediment-buried igneous oceanic crust. *Earth Planet. Science Lett.*, **146**, 137–150 (1997).

Fetter, C. W. Applied Hydrogeology (3rd ed.). Upper Saddle River, NJ. Prentice-Hall, 691 p. (1994).

Fisher, A. T. Rates and patterns of fluid circulation, in *Hydrogeology of the Ocean Lithosphere* (eds Davis, E. E. & Elderfield, H.). Cambridge University Press, New York (2004).

Fisher, A. T., Davis, E. E. & Becker, K. Borehole-to-borehole hydrologic response across 2.4 km in the upper oceanic crust: Implications for crustal-scale properties. *J. Geophys. Res.*, **113**, B07106 (2008).

Flueh, E. R., Fisher, M. A., Bialas, J., Childs, J. R., Klaeschen, D., Kukowski, N., Parsons, T., Scholl, D. W., ten Brink, U. S., Trehu, A. M. & Vidal, N. New seismic images of the Cascadia subduction zone from cruise SO108 – ORWELL. *Tectonophysics*, **293**, 69-84 (1998).

Freeze, R.A. & Cherry, J. A. Groundwater. Englewood Cliffs, NJ. Prentice-Hall, 604 p. (1979).

Fuis, G. S. West margin of North America – a synthesis of recent seismic transects. *Tectonophys.* **288**, 265-292 (1998).

Gerdom, M., Trehu, A. M., Flueh, E. R. & Klaeschen, D. The continental margin off Oregon from seismic investigations. *Tectonophysics*, **329**, 79-97 (2000).

Gullick, S. P. S., Meltzer, A. M. & Clarke Jr., S. H. Seismic structure of the southern Cascadia subduction zone and accretionary prism north of the Mendocino triple junction. *J. Geophys. Res.*, **103**, 27207-27222 (1998).

Hacker, B. R., Abers, G. A. & Peacock, S. M. Subduction factory 1. Theoretical mineralogy, densities, seismic wave speeds, and H2O contents. *J. Geophys. Res.*, **108**, 2029 (2003).

Harris, R. N., Spinelli, G., Ranero, C. R., Grevemeyer, I., Villinger, H. & Barckhausen, U. Thermal regime of the Costa Rican convergent margin: 2. Thermal models of the shallow Middle America subduction zone offshore Costa Rica. *Geochem. Geophys. Geosys.*, **11**, Q12S29 (2010).

Hyndman, R. D. & Wang, K. The rupture zone of Cascadia great earthquakes from current deformation and the thermal regime. *J. Geophys. Res*., **100**, 22133-22154 (1995).

Hyndman, R. D. & Wang, K. Thermal constraints on the zone of major thrust earthquakes failure: The Cascadia subduction zone. *J. Geophys. Res*., **98**, 2039-2060 (1993).

Hyndman, R. D., Wang, K. & Yamano, M. Thermal constraints on the seismogenic portion of the southwestern Japan subduction thrust. *J. Geophys. Res*., **100**, 15373-15392 (1995).

Kummer, T. & Spinelli, G. A. Hydrothermal circulation in subducting crust reduces subduction zone temperatures. *Geology*, **36**, 91-94 (2008).

McCaffrey, R. Time-dependent inversion of three-component continuous GPS for steady and transient sources in northern Cascadia. *Geophys. Res. Lett.*, **36**, L07304 (2009).

McCaffrey, R., Qamar, A. I., King, R. W., Wells, R., Khazaradze, G., Williams, C. A., Stevens, C. W., Vollick, J. J. & Zwick, P. C. Fault locking, block rotation and crustal deformation in the Pacific Northwest. *Geophys. J. Int.*, **169**, 1315-1340 (2007).

Moore, J. C. & Saffer, D. Updip limit of the seismogenic zone beneath the accretionary prism of Southwest Japan: An effect of diagenetic to low-grade metamorphic processes and increasing effective stress. *Geology*, **29**, 183-186 (2001).

Nicholson, T., Bostock, M. G. & Cassidy, J. F. New constraints on subduction zone structure in northern Cascadia. *Geophys. J. Int.*, **161**, 849-859 (2005).

Oleskevich, D. A., Hyndman, R. D. & Wang, K. The updip and downdip limits of great subduction earthquakes: Thermal and structural models of Cascadia, south Alaska, SW Japan, and Chile. *J. Geophys. Res*., **104**, 14965-14991 (1999).

Olsen, K. B., Stephenson, W. J. & Geisselmeyer, A. 3D crustal structure and long-period ground motions from a M9.0 megathrust earthquake in the Pacific Northwest region. *J. Seismology*, **12**, 145-159 (2008).

Pacheco, J. F. & Sykes, L. R. Seismic moment catalog for large shallow earthquakes from 1900 to 1989, *Bull. Seis. Soc*., **82**, 1306-1349 (1992).

Parsons, T., Trehu, A. M., Luegert, J. H., Miller, K., Kilbride, F., Wells, R. E., Fisher, M. A., Flueh, E. R., ten Brink, U. S. & Christensen, N. I. A new view into the Cascadia subduction zone and volcanic arc: implications for earthquake hazards along the Washington margin. *Geology*, **26**, 199-202 (1998).

Rogers, A. M., Walsh, T. J., Kockelman, W. J. & Priest, G. R. in *Assessing earthquake hazards and reducing risk in the Pacific Northwest* (eds Rogers, A. M., Walsh, T. J., Kockelman, W. J. & Priest, G. R) 1-54 (US Government Printing Office, Denver, 1996).

Rogers, G. & Dragert, H. Episodic tremor and slip on the Cascadia subduction zone: The chatter of silent slip. *Science*, **300**, 1942-1943 (2003).

Rondenay, S., Abers, G. A. & van Keken, P. E. Seismic imaging of subduction zone metamorphism. *Geology*, **36**, 275-278 (2008).

Satake, K. & Tanioka, Y. Souces of tsunami and tsunamigenic earthquakes in subduction zones. *Pure and Applied Geophysics*, **154**, 467-483 (1999).

Scholz, C. H. The Mechanics of Earthquakes and Faulting. Cambridge University Press, (2002).

Spinelli, G. A. & Wang, K. Effects of fluid circulation in subducting crust on Nankai margin seismogenic zone temperatures. *Geology,* **36**, 887-890 (2008).

Spinelli, G. A. & Wang, K. Links between fluid circulation, temperature, and metamorphism in subducting slabs. *Geophys. Res. Lett.*, **36**, L13302 (2009).

Trehu, A. Subsurface temperatures beneath southern Hydrate Ridge. *Proc. Ocean Drilling Prog. Sci. Res.*, **204**, 26pp. (2006).

Vrolijk, P. On the mechanical role of smectite in subduction zones. *Geology*, **18**, 703–707 (1990).

Wang, K. Applying fundamental principles and mathematical models to understand processes and estimate parameters, in *Hydrogeology of the Ocean Lithosphere* (eds Davis, E. E. & Elderfield, H.) 376-314 (Cambridge University Press, New York, 2004).

Wilson, D. S. Confidence intervals for motion and deformation of the Juan de Fuca Plate. *J. Geophys. Res.*, **98**, 16053-16071 (1993).